Draft version June 22, 2022
Typeset using LaTeX twocolumn style in AASTeX631

arXiv:2112.07871v3 [astro-ph.GA] 19 Jun 2022

The Compactness of Galaxy Groups in the Sloan Digital Sky Survey

Yun-Liang Zheng (郑云亮) [1,2] Shi-Yin Shen (沈世银) [1,3] and Shuai Feng(冯帅) [4,5]

[1] Key Laboratory for Research in Galaxies and Cosmology, Shanghai Astronomical Observatory, Chinese Academy of Sciences, 80 Nandan Road, Shanghai, China, 200030

[2] University of Chinese Academy of Sciences, No.19A Yuquan Road, Beijing, China, 100049

[3] Key Lab for Astrophysics, Shanghai, China, 200034

[4] College of Physics, Hebei Normal University, 20 South Erhuan Road, Shijiazhuang, 050024, China

[5] Hebei Key Laboratory of Photophysics Research and Application, 050024 Shijiazhuang, China

(Received 2021.10.28; Revised 2021.12.13; Accepted 2021.12.14)

Submitted to ApJ

ABSTRACT

We use an updated version of the halo-based galaxy group catalog of Yang et al., and take the surface brightness of the galaxy group ($\mu_{\rm lim}$) based on projected positions and luminosities of galaxy members as a compactness proxy to divide groups into sub-systems with different compactness. By comparing various properties, including galaxy conditional luminosity function, stellar population, active galactic nuclei (AGN) activity, and X-ray luminosity of the intra-cluster medium of carefully controlled high (HC) and low compactness (LC) group samples, we find that the group compactness plays an essential role in characterizing the detailed physical properties of the group themselves and their group members, especially for low mass groups with $M_h \lesssim 10^{13.5} h^{-1} M_\odot$. We find that the low-mass HC groups have a systematically lower magnitude gap Δm_{12} and X-ray luminosity than their LC counterparts, indicating that the HC groups are probably in the early stage of group merging. On the other hand, a higher fraction of passive galaxies is found in the HC group, which however is a result of systematically smaller halo-centric distance distribution of their satellite population. After controlling of both M_h and halo-centric distance, we do not find any differences for both the quenching faction and AGN activity of the member galaxies between the HC and LC groups. Therefore, we conclude that the halo quenching effect, which result in the halo-centric dependence of galaxy population, is a faster process compared to the dynamical relaxed time-scale of galaxy groups.

Keywords: keyword1 – keyword2 – keyword3

1. INTRODUCTION

In the paradigm of hierarchical structure formation, galaxies are believed form via baryonic gas cooling and condensation within dark matter halos. It is generally assumed that halo mass (M_h) is the most fundamental parameter that determines the evolutionary path of galaxies inside (e.g., Weinmann et al. 2006; Wetzel et al. 2012; Woo et al. 2013, 2015; Bluck et al. 2014, 2016; Wang et al. 2018; Davies et al. 2019). Based on this assumption, numerous models for linking galaxies to dark matter halos have been developed, such as the halo occupation distribution model (HOD, Jing et al. 1998; Peacock & Smith 2000; Zheng et al. 2005; Zu & Mandelbaum 2016), abundance matching model (HAM, Mo et al. 1999; Kravtsov et al. 2004; Vale & Ostriker 2006; Guo et al. 2010; Simha et al. 2012; Reddick et al. 2013), the conditional luminosity function (CLF, Yang et al. 2003, 2008; Cooray 2006; van den Bosch et al. 2007), and halo-based empirical models (Yang et al. 2013; Lu et al. 2014; Moster et al. 2018). In these models, dark matter halos have evolved hierarchically through repeated mergers. Galaxies that form the main branch of a merger tree generally reside near the halo center (Lange et al. 2018)

Corresponding author: Shi-Yin Shen
ssy@shao.ac.cn

and are referred to as central galaxies, while others that form in the sub-branch and orbit the central galaxies are referred to as satellite galaxies. These two galaxy populations have experienced different evolutionary paths so that their properties are different statistically as a result (e.g., Weinmann et al. 2006; van den Bosch et al. 2008; Peng et al. 2010; Knobel et al. 2015; Davies et al. 2019).

From an observational point of view, the physical properties of galaxies are strongly correlated with their stellar mass ($M_\star$) and environment (e.g., Dekel & Birnboim 2006; Peng et al. 2010, 2012, 2014; Liu et al. 2019; Zhang et al. 2021). Specific mechanisms have been proposed for mass dependency, including supernovae and active galactic nuclei (AGN) feedback (Croton et al. 2006; Fabian 2012; Harrison 2017), while the physical mechanisms of the environmental effects on the dwarf/satellite galaxies include tidal interaction (Farouki & Shapiro 1981), ram-pressure stripping (Gunn & Gott 1972), and harassment (Moore et al. 1996), etc. In the framework of halo model, the observed environmental effects of galaxies can be interpreted as a dependence on their host halos (e.g., Liu et al. 2010; Wetzel et al. 2012; Henriques et al. 2017; Wang et al. 2018; Davies et al. 2019). Indeed, Haas et al. (2012) demonstrate that the environmental parameters of galaxies defined in a traditional way (e.g., projected local density, projected distance to the ith nearest galaxy, etc.) are in effect measures of their host halo mass M_h. However, there are also observational indications that galaxies exhibit more complex environmental effects beyond the simple M_h model. For example, More et al. (2011) and Mandelbaum et al. (2016) revealed that the stellar-to-halo mass relation is further correlated with the physical properties of central galaxies. From an evolutionary point of view, dark matter halos form via mergers of smaller halos. When dark matter halos merge, infalling galaxies do not necessarily merge with central galaxies in a short timescale but keep orbiting and interacting with the central galaxies (Stewart et al. 2009). Therefore, in addition to M_h, the halo formation time (or the assembly history) has long been used as the second parameter to profile the dark matter halos when analyzing the simulation data (e.g., Matthee et al. 2017; Zehavi et al. 2018; Cui et al. 2021).

In observation, the host M_h of galaxy systems can be estimated from the total stellar mass or richness of the group members (e.g., Yang et al. 2005, 2007, 2021; Robotham et al. 2011). However, it is not clear how to link the observational properties of galaxy groups to their assembly history. Several studies on fossil groups of galaxies (e.g., Dariush et al. 2010; Raouf et al. 2014, 2018; Khosroshahi et al. 2017; Li & Cen 2020) have suggested that Δm_{12}, the magnitude gap between the first and second brightest members, might characterize the assembly history of a galaxy group. However, recent studies (e.g., Shen et al. 2014; Trevisan & Mamon 2017) have shown that the origin of large Δm_{12} is quite complex and cannot be simply accounted for by the halo formation time. On the other hand, like the size of galaxies, the size (or compactness) of galaxy groups might be another observationally accessible parameter encoding the assembly histories of halos. Indeed, it has long been known that there is a special class of galaxy groups, compact groups of galaxies (CGs), which is defined as a group system containing a few galaxies separated by distance of an order of galaxy size (e.g., Hickson 1982; Barton et al. 1996; Díaz-Giménez & Zandivarez 2015; Sohn et al. 2015, 2016; Díaz-Giménez et al. 2018; Zheng & Shen 2020). Because of the observational facts that tidal interactions and mergers frequently appear among CG members, (e.g., Barnes 1989; Amram et al. 2004; Coziol & Plauchu-Frayn 2007; Torres-Flores et al. 2009, 2010, 2014), CGs are believed to represent the sites for massive members that are about to merge. Moreover, based on simulation, Farhang et al. (2017) suggested that CGs are early-formed systems that depart from ordinary hierarchical assembly and stressed that CGs appear to be a distinct halo environment. Inspired by the ideas about the peculiarity of CGs, several comparative studies on the galaxy properties of CGs and non-CGs have been performed. For instance, Coenda et al. (2012) showed that CGs contain a larger fraction of red, early-type galaxies in comparison to loose groups and fields at a given absolute magnitude, while Cluver et al. (2020) found no significant difference in the scale relation between quenched fraction and $M_\star$ in group systems with different levels of compactness.

The connection between the observational selected CGs and halo-model-based groups has been recently investigated by Zheng & Shen (2021). In that study, we show that the observationally selected CGs are physically heterogeneous systems and can be mainly separated into two categories, the isolated systems and those embedded in rich groups or clusters. For these isolated CGs, we find that they have lower dynamical masses compared to the non-compact ones at the same group luminosity. However, we cannot distinguish whether this lower dynamical mass state is a result of a merging process or the dynamical evolution of post-mergers. In this paper, we expand our studies on CGs (Zheng & Shen 2020, 2021) and for the first time, take the compactness of galaxy groups as a general parameter to explore its correlations with other physical properties of galaxy groups and group members when M_h is

controlled. Moreover, since the X-ray emission from the intragroup medium contains rich information on the dynamical status of galaxy groups, for the first time, we also compare the X-ray properties of galaxy groups with different compactness using a statistical method in this study. Our goal is to figure out whether the group compactness plays a role as a second observational parameter in describing the properties and merger histories of galaxy groups.

This paper is organized as follows. We describe the halo-based group samples in Section 2, and the measurements of relevant properties in section 3. We present our results for the global and individual properties of groups with different compactness in section 4 and 5, respectively. We provide a brief discussion in Section 6 and summarize our conclusions in Section 7. Throughout this paper, we assume a flat ΛCDM cosmology with parameters: $\Omega_m = 0.27$ and $H_0 = 100h$ km s^{-1} Mpc^{-1} with $h = 0.7$.

2. SAMPLE: GROUPS OF GALAXIES

In this work, we take use of the group catalog of Yang et al. (2007, 2012, hereafter Y07), which has been derived from the latest version of New York University Value-Added Galaxy Catalog (VAGC, Blanton et al. 2005) based on the SDSS legacy survey (Abazajian et al. 2009) with a set of improved reduction. Y07 has applied a halo-based group finder to assign each galaxy in the SDSS-DR7 Main Galaxy Sample (MGS) within the redshift range of $0.01 < z < 0.20$ and r-band magnitude brighter than 17.72 mag to a unique group. In Y07, three versions of a group catalog have been constructed based on different redshift sources. In this work, we use sample III of the Y07 group catalog containing $\sim 640,000$ galaxies, where a small fraction of the members ($\sim 37,000$) without spectroscopic redshifts have been assigned with the redshifts of their nearest neighbors. Therefore, sample III of the Y07 group catalog has 100% completeness of member galaxies, while it also contains contamination from background or foreground galaxies.

Since $\sim 13,000$ out of $\sim 37,000$ spectroscopically unmeasured galaxies have achieved new redshifts from SDSS-DR16 (Ahumada et al. 2020), GAMA-DR2 (Liske et al. 2015), and LAMOST-DR7 (Luo et al. 2015), the contamination of the group catalog can be significantly reduced (e.g., Shen et al. 2016; Feng et al. 2019; Zheng & Shen 2020). Here, we use these new redshift measurements to update the sample III of the Y07 group catalog. We find ~ 8500 out of $\sim 13,000$ galaxies with new redshift measurements are concordant with their nearest neighbors, thus, their group ID remains unchanged. For the remaining ~ 4500 galaxies having updated redshifts but inconsistent with their nearest neighbors, we reassign them to a particular group following the criteria of Y07 and update the original halo properties accordingly. For the remaining $\sim 24,000$ out of $\sim 37,000$ galaxies without new redshift detection, we keep them unchanged.

Owing to our aim of investigating how group properties vary with group compactness, which is defined based on at least three members, we only consider $N \geq 3$ groups in this work. Moreover, we have also noticed that bad photometry (e.g., one large extended galaxy deblending into various small pieces or a fragment of a satellite trail identified as a chain of several galaxies, McConnachie et al. 2009; Zheng & Shen 2020) will contaminate the following results because these problematic sources are more likely to be identified as groups with higher compactness. Therefore, we have made visual inspections of the images of the $N \geq 3$ groups and removed ~ 300 fake detections, most of which belong to low M_h groups.

Y07 has estimated the characteristic stellar mass ($M_{19.5}$) and luminosity ($L_{19.5}$) of each group by summing up the masses and luminosities of all the members with ${}^{0.1}M_r - 5\log h \leq -19.5$ mag, respectively. For the distant groups ($z > 0.09$) where the corresponding faint-end limit brighter than ${}^{0.1}M_r - 5\log h = -19.5$ mag, their $M_{19.5}$ and $L_{19.5}$ have been corrected for the missing members. Y07 has also estimated two versions of M_h for each group based on their $M_{19.5}$ or $L_{19.5}$, respectively. Unless stated otherwise, we adopt the values based on $M_{19.5}$ as recommended in Y07 paper. For some groups, their M_h have been updated due to the slight revision of their group membership, especially for those groups containing the galaxies with discordant new redshifts. There are also ~ 700 $N \geq 3$ groups without M_h calculated because none of their members is brighter than ${}^{0.1}M_r - 5\log h \leq -19.5$ mag, thus we remove them in the following analysis.

Finally, there are 22,468 $N \geq 3$ groups with M_h assigned, which have 140,930 member galaxies and 129,622 of them ($\sim 92\%$) have spectroscopic redshifts. The lower redshift completeness of the final sample compared to the overall galaxy sample ($\sim 95\%$) is caused by the fact that almost all of the galaxies with assigned redshifts are members of $N \geq 2$ systems.

In Y07, the dark matter halos are defined as having an over-density of 180, we recompute the halo radius (R_{180}) and group velocity dispersion (σ) given by the Equation (5) and (6) in Y07 paper due to the revision of M_h estimate. Unless stated otherwise, the central galaxy of each group are identified to be the most massive one.

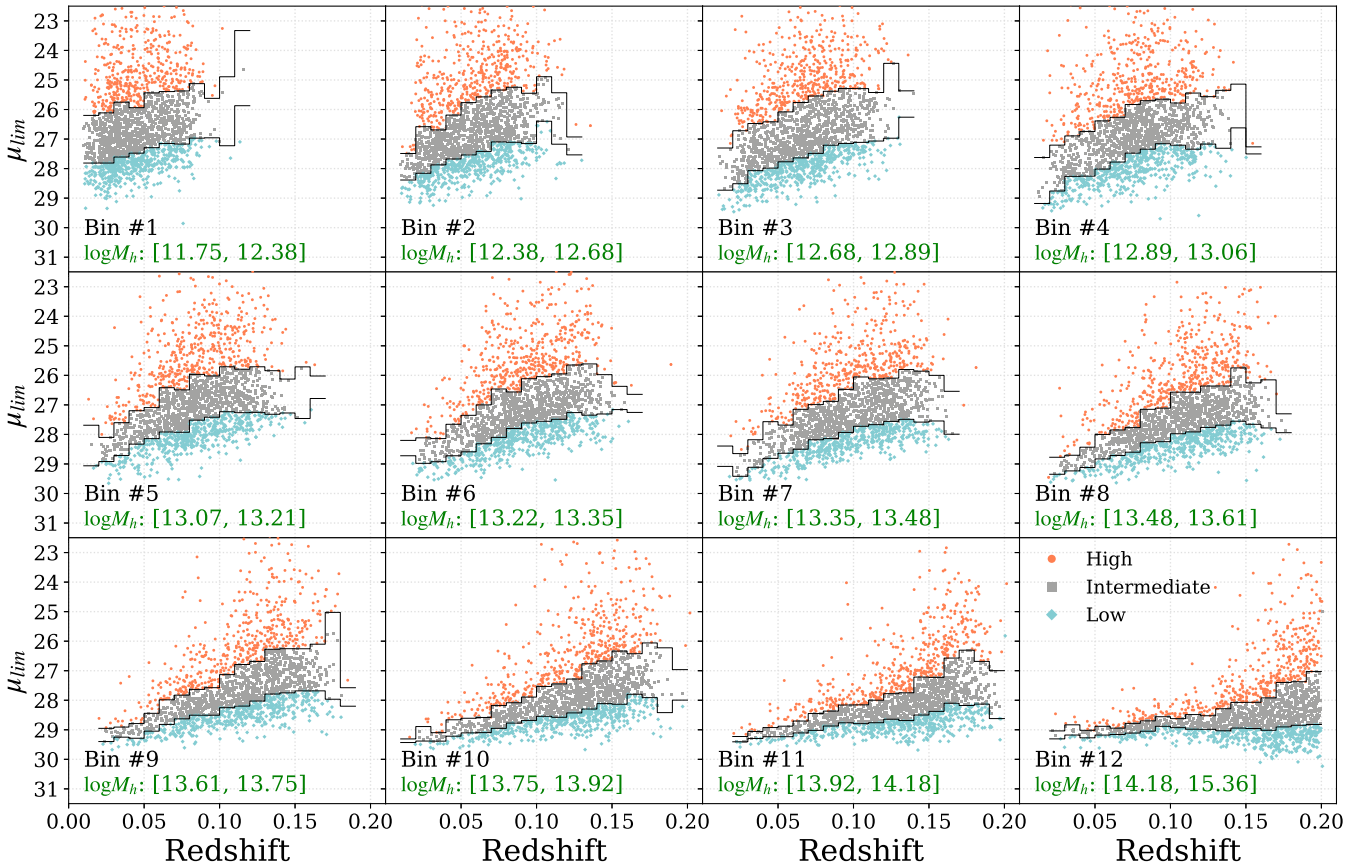

Figure 1. The $\mu_{\rm lim}$−redshift diagrams for groups in different M_h bins. The bin number and mass range of M_h are given in the lower-left corner of each subplot. The solid step lines in each subplot represent the 25th and 75th percentiles of the $\mu_{\rm lim}$ in each redshift bin with a bin size of 0.01. The data points above the upper step lines are regarded as HC groups (red circle), those lying in the middle are regarded as IC groups (grey square), and those below the lower step lines are LC groups (blue diamond).

2.1. *Compactness of galaxy groups*

In this work, we use the group surface brightness as a proxy for group compactness. Following Hickson (1982), the surface brightness of a group system is defined as:

$$\mu_{\rm lim} = -2.5 \log \left(\frac{\sum_{i=1}^{N} 10^{-0.4 m_i}}{\pi \theta_{\rm G}^2} \right), \qquad (1)$$

where $\mu_{\rm lim}$ is the surface brightness averaged over the smallest circle enclosing N galaxy members brighter than the magnitude limit within an angular radius of $\theta_{\rm G}$ in units of arcseconds, and m_i is the apparent magnitude of the ith brightest member.

To fairly define the compactness level of galaxy groups, we divide the groups into 12 M_h bins with equal sample size and then plot $\mu_{\rm lim}$ against redshift for each M_h bin in figure 1. For each M_h bin, we further divide groups into 20 redshift bins with a bin width of 0.01, and then calculate the 25$^{\rm th}$ and 75$^{\rm th}$ percentile values of $\mu_{\rm lim}$ distribution in each redshift bin. The solid lines in each panel of figure 1 show the separation lines of the 25$^{\rm th}$ and 75$^{\rm th}$ percentiles, respectively. We see that there is a systematical redshift dependence of $\mu_{\rm lim}$ quartiles, where the higher redshift groups are biased toward higher $\mu_{\rm lim}$ values. This redshift bias is likely caused by the segregation effect of galaxies with different masses (see section 6 for a detailed discussion).

Here, we are not interested in well-defining the compactness of groups of galaxies with a quantitative $\mu_{\rm lim}$ criterion. On the contrary, our aim is to make a fair comparison of galaxy groups with different compactness while their other main physical features are well constrained. To do that, we consider the groups of each M_h bin that lie in the top quartile to be high compactness (HC) groups, while those lying in the middle two quartiles are considered as intermediate compactness (IC) groups and those in the bottom quartile are considered to be low compactness (LC) groups. With this configuration, our HC and LC groups have the same M_h and

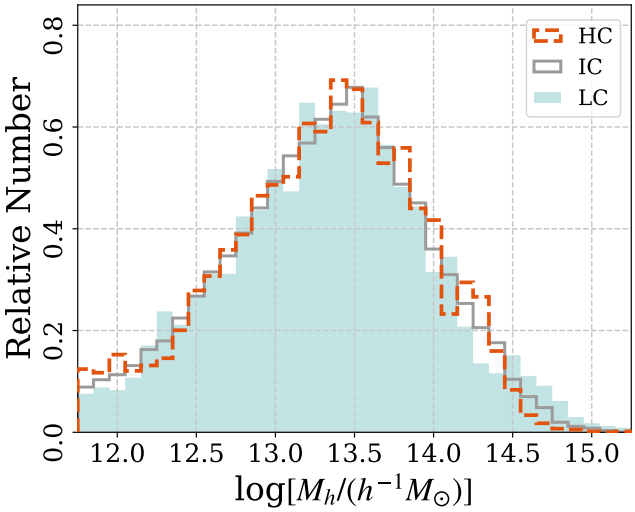

Figure 2. The M_h distributions for the HC (red dashed), IC (grey solid), and LC (blue filled) groups with a bin width of 0.1 dex.

redshift distribution, and thus any differences in between these two samples would mainly correlate with the compactness of galaxy groups. In figure 2, we show the M_h distribution of the Y07 groups with different levels of compactness. As expected, these three different samples have nearly the same M_h distributions, which peaks around $\sim 10^{13.5}h^{-1}M_\odot$.

Moreover, for the $M_h \lesssim 10^{13.5}h^{-1}M_\odot$ groups, the separation line of the top quartile is close to the criterion $\mu_{\rm lim} \sim 26.0$ mag arcsec^{-2} that is used for defining the compact groups of galaxies (Hickson 1982). That is to say, there might be a good correspondence between the classical compact groups and our low-mass HC groups. On the other hand, for high-mass systems ($M_h \gtrsim 10^{13.5}h^{-1}M_\odot$), the majority of the groups in the high compactness quartiles are actually not 'compact' enough ($\mu_{\rm lim} > 26.0$ mag arcsec^{-2}).

2.2. *X-ray emission of galaxy groups*

We perform X-ray detections for Y07 groups in the *ROSAT* All Sky Survey (RASS) image data, which mapped the sky in the soft X-ray band ($0.1-2.4$ keV) with exposure time varying between 400 and 40000 seconds, depending on the direction in the sky. The resolution of the RASS images is 45 arcsec.

The algorithm we use to estimate the X-ray luminosity is similar to those of Shen et al. (2008) and Wang et al. (2014). As the first step, we determine the X-ray center of each group. Optically, the position of the central galaxy is usually taken to define the group center. Indeed, the X-ray peak position might be offset from the central galaxy (e.g., Dai et al. 2007; Koester et al. 2007; Shen et al. 2008; Wang et al. 2014). We locate the RASS fields where the group reside, then apply a maximum-likelihood (ML) search algorithm to generate the X-ray source catalog with detection likelihood $L > 7$ in the $0.5-2.0$ keV band (Voges et al. 1999). We match all the detected sources within a tolerance of $0.1R_{180}$ from the central galaxies and regard the closest one as the X-ray center. The other X-ray sources within $0.1R_{180}$ are regarded as part of the extended X-ray emission from this group, and those that lie in $R > 0.1R_{180}$ region are regarded as a contaminated source that are not associated with the emission of intra-group medium. If none of the X-ray sources is detected within $0.1R_{180}$, the central galaxy then is regarded as the X-ray center, most of our samples ($\sim 90\%$) belong to such cases.

To obtain an unbiased estimate of the typical X-ray luminosity of a subset of galaxy groups, we stack each subsample with similar M_h and group compactness. The stacking method is described in Shen et al. (2008). Briefly, we center each group image on the X-ray center. All the images are scaled to the same size in units of R_{180} and the contaminated sources located at $R > 0.1R_{180}$ are masked out. The X-ray background is estimated as the average flux inside an annulus with inner radius of R_{180} and outer radius of $1.3R_{180}$. By subtracting the background, a one-dimensional count rate profile as a function of radius is then obtained.

For a stack of N groups, the source count of photons, $N_{\rm S}$, that could be detected in RASS is given as

$$N_{\rm S} = \sum_{i=1}^{N} L_{{\rm X},i}\, g\left(N_{{\rm H},i}, T_i, z_i\right) t_i, \qquad (2)$$

where $L_{\rm X,i}$ is X-ray luminosity of the ith group, t_i is average RASS effective exposure time of ith group, and $g\left(N_{\rm H,i}, T_i, z_i\right)$ is a coefficient converting bolometric X-ray luminosity to observed count rate as functions of redshift z_i, average galactic hydrogen column density $N_{\rm H,i}$ in the line of sight and gas temperature within the ith group. We assume that the gas metal abundance is assumed to be 0.3 of the solar value, whereas $N_{\rm H,i}$ is taken from the map of Dickey & Lockman (1990) and the X-ray emission has a thermal spectrum with temperature T obtained from the empirical $T-\sigma$ scaling relation of White et al. (1997). However, the slope of the $T-\sigma$ relation for small groups is not necessarily the same as massive clusters, and the gas temperature of low M_h groups is even not well-constrained (Lovisari et al. 2021, and references therein). Moreover, the conversion factor for hot gas with $T \lesssim 0.3$ keV (corresponding to $M_h \lesssim 10^{13}h^{-1}M_\odot$) becomes very different for different X-ray spectral models (e.g., power law, thermal bremsstrahlung, Raymond-Smith plasma, and blackbody spectrum) over this range (Briel et al. 1996).

However, until there is more negative evidence, there is reason to believe that the $N_{\rm H}$ and T distributions for groups at fixed M_h but with different compactness are similar, i.e., they have similar $g\left(N_{\rm H,i}, T_i, z_i\right)$ distributions. Indeed, we have checked that the difference between the resulting X-ray luminosity of the LC groups and HC ones (we will show in figure 6) is caused by the difference between their detected X-ray photon counts rather than the specific values of the conversion factor $g\left(N_{\rm H,i}, T_i, z_i\right)$.

For simplicity, we use the conversion factors given by the table 2, 3, and 5 of (Böhringer et al. 2004). For the groups with gas temperature below the lowest threshold of each table, we take use of the values in that row. Based on the assumption that the X-ray luminosities of the sources in a stack are similar, the weighted average X-ray luminosity, $L_{\rm X,S}$, of the stack can be given as

$$L_{\rm X,S} = \frac{N_{\rm S}}{\sum\limits_{i=1}^{N} g\left(N_{{\rm H},i}, T_i, z_i\right) t_i}, \tag{3}$$

Following Wang et al. (2014), the X-ray extension radius is set as a fixed value of $R_{\rm X} = 0.5R_{180}$ and the source count rates are integrated into the X-ray extension radius R_X. By changing this fixed value from $R_{\rm X} = 0.3R_{180}$ to $0.6R_{180}$, none of our main results is significantly impacted. Finally, to estimate the flux that is missed outside $R_{\rm X}$, we make a $\beta-$profile extension correction to make up the X-ray luminosity missed in the range $R_{\rm X} \leq R \leq R_{180}$ (see Böhringer et al. 2000; Shen et al. 2008; Wang et al. 2014) with $\beta = 2/3$ and core radius $R_c = 0.14R_{180}$. If β is set as a free parameter in profile fitting, we find all the best fittings are in the range of $0.40 - 0.70$, but with large uncertainties. Therefore, we use a fixed value of β to make the profile fitting and flux calibration.

3. SAMPLE: PHYSICAL PROPERTIES OF GROUP MEMBER GALAXIES

3.1. *Quenched and Star-forming Galaxies*

The $M_\star$ and star formation rate (SFR) of individual galaxies are directly retrieved from the MPA/JHU-DR7 release (Brinchmann et al. 2004; Kauffmann et al. 2003) based on SDSS spectroscopy. There are $\sim 123,000$ out of $(140,930)$ galaxies in our sample have been detected. These galaxies without match in MPA/JHU catalog are mainly caused by the fiber collision effect during the SDSS spectroscopy target. In other words, their redshifts is obtained from other surveys rather than SDSS-DR7. Due to the need for determining central galaxies, the $M_\star$ of these unmeasured galaxies are obtained by the relation between stellar mass-light ratio and $(g-r)$ colors of Bell et al. (2003). Following Li et al. (2006), the catastrophic $(g-r)$ color outside the 3σ ranges from the mean color-magnitude relations of both blue and red sequences is replaced by the mean color of the red or blue cloud, depending on their location on the diagram.

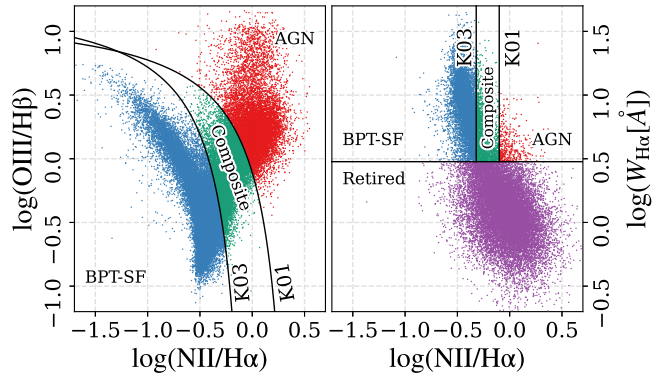

Figure 3. Classification of spectral types for strong- and weak-line galaxies in Y07 groups. Left Panel: The BPT diagnostic diagram for strong-line galaxies with [O III]/Hβ versus [N II]/Hα emission-line ratios. The demarcation lines are taken from Kewley et al. (2001, K01) and Kauffmann et al. (2003, K03). Right Panel: The WHAN diagram for weak-line galaxies in Y07 groups. The SF/composite/AGN demarcation lines are transposed from K01 and K03, respectively (Cid Fernandes et al. 2010), and the retired/non-retired demarcation line is taken from Cid Fernandes et al. (2011).

Based on the bimodality of galaxies distributed in the SFR $- M_\star$ diagram, galaxies can be divided into star-forming and quenched population. We adopt the demarcation line suggested by Bluck et al. (2016), which is parallel to but 1 dex below the star formation main sequence:

$$\log {\rm SFR} = 0.73 \log M_\star - 1.46 \log h - 8.3, \tag{4}$$

where the reduced Hubble constant h is included here to convert the units of $M_\star$ from $M_\odot$ used in Bluck et al. (2016) to $h^{-2}M_\odot$ used here. We have also examined the results based on the demarcation line given by Woo et al. (2013), and find negligible changes.

3.2. *AGN classification*

3.2.1. *Optical AGNs*

The emission lines related to AGN classification are also taken from the MPA/JHU catalog. The optical AGN are classified based on the BPT diagram (Baldwin et al. 1981), which is traditionally used to separate type II AGN from star-forming and composite galaxies. Here, we use the demarcation lines proposed by Kewley et al. (2001) and Kauffmann et al. (2003) (the left panel of figure 3). Following Pasquali et al. (2009), the fluxes

of the four emission lines are required to have a signal-to-noise ratio of S/N ≥ 3. This results in a sample of $\sim 50,000$ AGN out of $\sim 123,000$ strong-line galaxies. Besides, there are $\sim 28,000$ weak-line galaxies whose Hα and [N II] lines are both detected with an S/N ≥ 3, but either or both of Hβ and [O III] lines have a lower S/N. Then, following Cid Fernandes et al. (2010, 2011), we use the WHAN method, which only requires [N II]/Hα and Hα equivalent width ($W_{\rm H\alpha}$) to select weak-line AGN. We show the classification diagram for weak-line galaxies in the right panel of figure 3. Note that the emission line fluxes have been corrected for intrinsic extinction based on the Balmer decrement and a dust attenuation curve of the form $\lambda^{-0.7}$ (Charlot & Fall 2000) by assuming an intrinsic Hα/Hβ = 2.86 (Osterbrock 1989).

3.2.2. *Radio-loud AGN*

Radio-loud AGNs are obtained by matching our sample galaxies with the radio galaxy catalog of Best & Heckman (2012), which was established by cross-matching the MPA/JHU catalog with the NVSS (National Radio Astronomy Observatory Very Large Array Sky Survey, Condon et al. 1998) and FIRST (Faint Images of the Radio Sky at Twenty centimeters, Becker et al. 1995) surveys following the method of Best et al. (2005). The catalog is down to a flux density level of 5 mJy, which means that the catalog probes down to a radio luminosity of $L_{1.4\rm GHz} = 10^{23}{\rm W\cdot Hz^{-1}}$ at $z = 0.1$, we thus only consider the galaxies with $z \leq 0.1$ (Wang et al. 2018) when investigating the radio-loud AGN fraction.

4. THE GLOBAL PROPERTIES OF GALAXY GROUPS: DEPENDENCE ON GROUP COMPACTNESS

In this section, we start with a detailed investigation of how the global properties of a galaxy group varied with the group compactness.

4.1. *CLFs*

The dynamical state of a group system is directly related to the luminosity distribution of its galaxy members (Martínez & Zandivarez 2012). As the first step in our investigation of how the group properties varied with group compactness, we use the CLF to describe the luminosity distribution of galaxies in groups with different levels of compactness at a given M_h. Following Yang et al. (2008), the total CLF can be modeled as the sum of the CLFs of central and satellite galaxies [1]:

$$\Phi\left({}^{0.1}M_r|M_h\right) = \Phi_{\rm cen}\left({}^{0.1}M_r|M_h\right) + \Phi_{\rm sat}\left({}^{0.1}M_r|M_h\right), \tag{5}$$

The CLF of central galaxies is assumed to be a lognormal form:

$$\Phi_{\rm cen}\left({}^{0.1}M_r|M_h\right) \propto \exp\left[-\frac{\left({}^{0.1}M_r - M^\star_{\rm cen}\right)^2}{2{\sigma^\star_{\rm cen}}^2}\right], \tag{6}$$

where $M^\star_{\rm cen}$ is the expected value for the absolute magnitude of the central galaxy, and $\sigma^\star_{\rm cen}$ is the standard deviation of $M^\star_{\rm cen}$. The CLF of satellite galaxies takes a modified Schechter (1976) function:

$$\begin{aligned}\Phi_{\rm sat}\left({}^{0.1}M_r|M_h\right) \propto & 10^{-0.4(\alpha^\star_{\rm sat}+1)\left({}^{0.1}M_r - M^\star_{\rm sat}\right)} \\ & \cdot \exp\left[-10^{-0.8\left({}^{0.1}M_r - M^\star_{\rm sat}\right)}\right],\end{aligned} \tag{7}$$

where $M^\star_{\rm sat}$ is the characteristic magnitude and $\alpha^\star_{\rm sat}$ is the faint-end slope of the satellite galaxies. Here, we focus on the shape of these CLFs only, and the parameters ($M^\star_{\rm cen}$, $\sigma^\star_{\rm cen}$, $M^\star_{\rm sat}$, and $\alpha^\star_{\rm sat}$) of CLFs are obtained using ML estimator (Tammann et al. 1979), where the binned CLFs are obtained via nonparametric stepwise maximum likelihood method (Efstathiou et al. 1988). The results for each parameter as a function of M_h are shown in figure 4, where we also plot an example of the fitting for the subsamples in M_h Bin = 5 derived via both methods to show the consistency of the results.

For central galaxies, we see that there is a strong dependence of CLF shape on M_h values. However, for a given M_h, there is only a weak dependence of CLF parameters on group compactness. For high M_h bins ($M_h \gtrsim 10^{13}h^{-1}M_\odot$), the three categories of galaxy groups with different compactness have almost identical $M^\star_{\rm cen}$ values. However, for low M_h bins ($M_h \lesssim 10^{13}h^{-1}M_\odot$), LC groups tend to have slightly but systematically brighter $M^\star_{\rm cen}$ than the others. The scatter of central galaxies $\sigma^\star_{\rm cen}$ are consistent with each other inside uncertainties for all M_h bins.

For the CLFs of satellite galaxies, we see not only a strong dependence on M_h, but also an obvious dependence on group compactness. The $M^\star_{\rm sat}$ of the LC groups is systematically fainter, while their faint-end slope, $\alpha^\star_{\rm sat}$, is more negative and hence contains more faint galaxy members than the HC groups. These two results are not independent of each other because there is a degeneracy between $M^\star_{\rm sat}$ and $\alpha^\star_{\rm sat}$ in modified

[1] In this section, we take the brightest galaxy in the group as the central galaxies instead of the most massive one. Tests have shown that both of the definitions yield indistinguishable results.

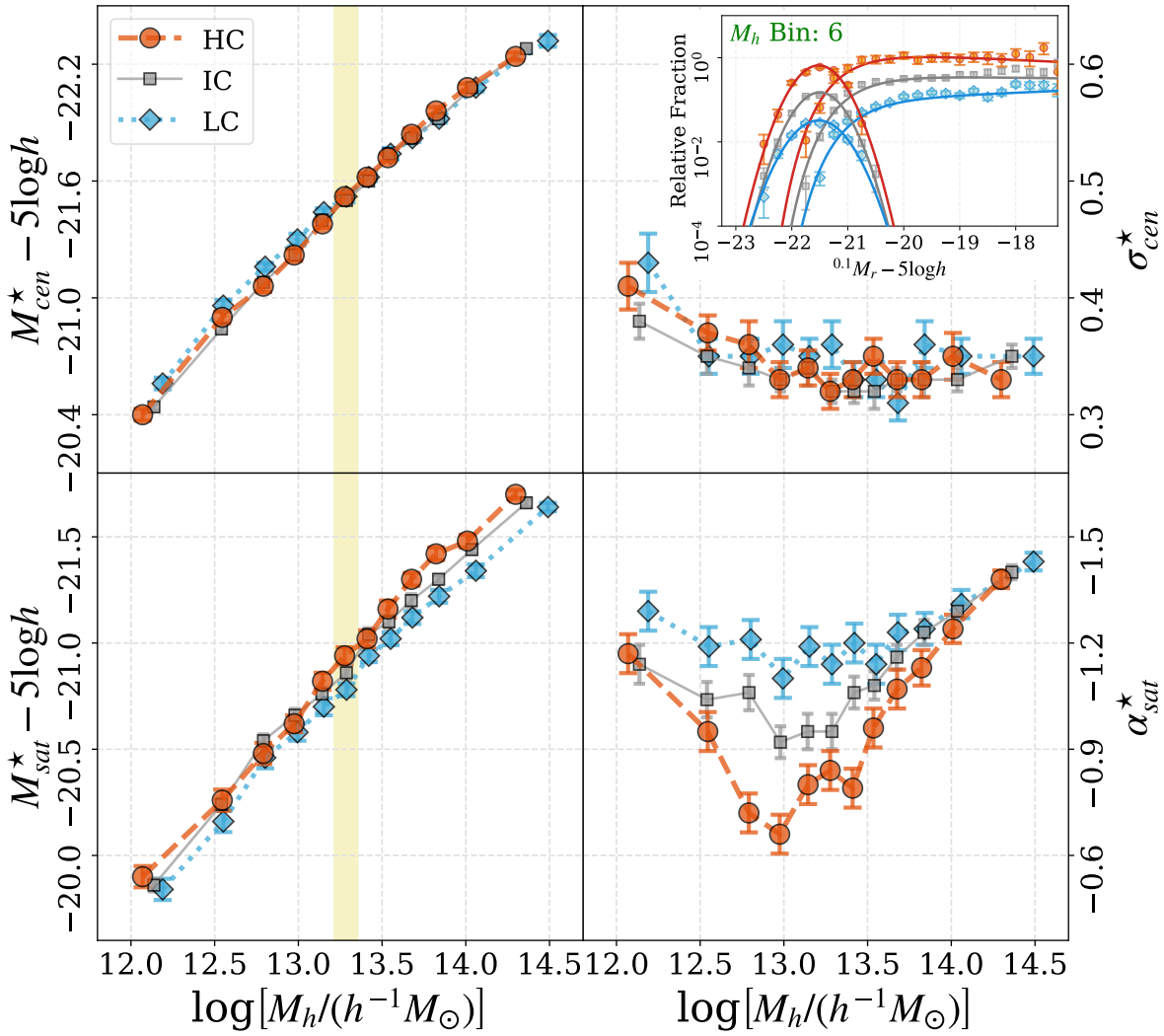

Figure 4. The best-fit parameters ($M^\star_{\rm cen}$, $\sigma^\star_{\rm cen}$, $M^\star_{\rm sat}$, and $\alpha^\star_{\rm sat}$) of CLFs for the HC (red), IC (grey), and LC (blue) groups as a function of M_h. The vertical error bars show the errors of the parameter in each M_h bin. The plot in the inset in the upper right corner demonstrates an example of a CLF fitting for the groups in M_h Bin = 6 (shaded region) derived via both a nonparametric stepwise (symbols with error bars) and parametric ML estimator (solid lines), the fitting for each subsample is manually shifted for clarity.

Schechter function fitting when the total luminosity is fixed. Besides, at a fixed total luminosity, groups with more galaxy members (so that more negative $\alpha^\star_{\rm sat}$) might also be biased toward having higher $\mu_{\rm lim}$ values (because of the larger radius of the smallest enclosed circle). To check to what extent the difference of richness between the LC and HC groups at a given M_h can explain the observed difference of $\mu_{\rm lim}$ values, we perform a simple test. More specifically, for a group with N members at a given M_h, we take the median θ_G of the observed samples as satisfying the conditions as expected at the radius $R_{\rm m}(N, M_h)$. By assuming the total luminosity of each group at a fixed M_h are the same, we thus can estimate the relative difference in $\mu_{\rm lim}$ distributions for the mock groups with the richness distribution assigned from HC and LC groups, respectively. Indeed, the disparity of the richness between the LC and HC groups at a given M_h can only explain at most $\sim 20\%$ of their $\mu_{\rm lim}$ difference.

4.2. *Luminosity gap:* Δm_{12}

The CLF results presented in the last section imply that the HC groups (especially for those with $M_h < 10^{13.5} h^{-1} M_\odot$) are biased to have fainter central galaxies and brighter satellites. Therefore, the natural conclusion is that the HC groups would be biased to have lower magnitude gap Δm_{12}. In this subsection, we investigate in detail how Δm_{12} is correlated with the group compactness.

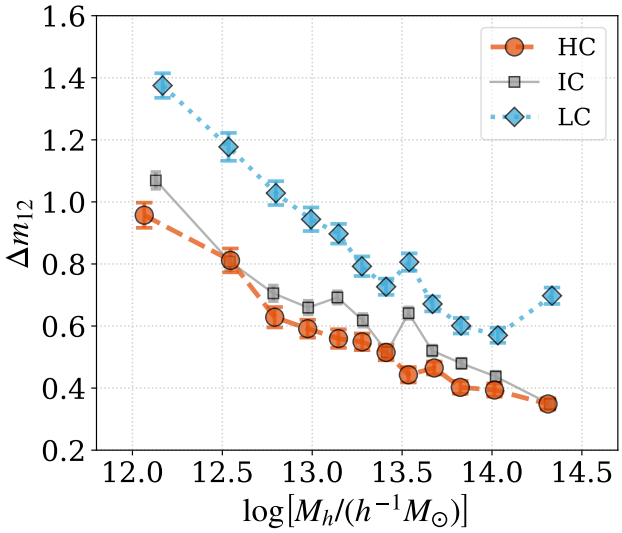

Figure 5. The median Δm_{12} as a function of M_h for the HC (red), IC (grey), and LC (blue) groups. The vertical error bars show the errors of the median Δm_{12} in each M_h bin. Note that the HC, IC, and LC groups in each M_h bin have been controlled to have similar redshift and richness distributions.

Based on the principle of order statistics, Shen et al. (2014) have shown that Δm_{12} is mainly determined by group richness, where groups with more members would be naturally biased to have smaller Δm_{12}. On the other hand, for groups with a given M_h, Δm_{12} has long been conjectured to reflect their dynamical states (e.g., More 2012; Paranjape & Sheth 2012; Tal et al. 2012). This argument is based on the fact that the dynamic friction drives massive major pairs to merge more quickly than other mergers within the same halo. The massive satellites would be coalesced by the central galaxies earlier, which drives Δm_{12} to increase with time. However, this simple scenario might not be enough to account for the observed $\Delta m_{1,2}$ of galaxy groups since all galaxy systems are in hierarchical merging and a recent merging event of group systems may significantly change Δm_{12} (Trevisan & Mamon 2017).

To perform a fair comparison of Δm_{12} between the groups with different compactness, we do not compare their Δm_{12} distribution in a straightforward way. We match the LC (IC) groups to the HC groups at the same M_h bin against the confounding covariates, $X = \{N, z\}$. We search for the counterparts within a distance of 1 scaled by a tolerance of $\{\Delta N, \Delta z\} = \{0, 0.01\}$ in the multi-dimensional space formed by X. We select the closest one (two, for IC groups) of them not selected yet. If all of the satisfied targets have been selected before, we pick the closest one again. If none of the targets satisfy the criterion, this HC group will be discarded.

Figure 5 shows the median Δm_{12} for the HC, IC, and LC groups in each M_h bin. Here we see that Δm_{12} decreases with increasing M_h, mostly due to the richness being generally higher for massive groups. On the other hand, the LC groups exhibit systematically larger Δm_{12} than the HC groups. This result confirms the conclusion we have obtained from the CLFs in the last section, which is also consistent with the fact that classical compact groups are generally comprised of several relatively more luminous/massive galaxies close in proximity to one another.

This result also raises a question on the dynamical status of the HC groups. Previous studies have suggested that galaxy groups show similar dynamical features (velocity dispersion, mean harmonic separation, and dynamical mass) in the late collapse and dynamical friction phases, although the time interval between these two phases is up to several gigayears (Mamon 1993, 2007; Zheng & Shen 2021). Hence, there are two possibilities for these observed HC groups, one is that the HC groups are dynamical young systems in the late forming stage, and the other is that they are dynamical old systems in late merging stage. Obviously, the systematically smaller Δm_{12} for the HC groups is much more likely to favor the former scenario. To further verify this hypothesis, we investigate the X-ray properties of groups with different compactness in the next section.

4.3. *X-ray Luminosities of Galaxy Groups*

In this section, we investigate how the average X-ray luminosity of galaxy groups depend on the group compactness. To increase the statistical significance of our results, we rebin each pair of the adjacent M_h bins in the following. We stack the groups of similar M_h and compactness independently. In figure 6, we present the average X-ray luminosity given by equation 3 as a function of M_h for the stacks of each subsample and show an example surface brightness profiles for the stacks of the HC and LC groups in M_h Bin $= 5 - 6$. As one can see, the S/N of the surface brightness profile is sufficiently good and can be well represented by the $\beta-$model.

Broadly, the X-ray luminosity of galaxy groups has a good correlation with M_h, in agreement with the results of Mantz et al. (2010) and Wang et al. (2014). Note that the X-ray luminosity and halo mass are defined in a different way in Mantz et al. (2010), we transform both of the quantities using the method following Wang et al. (2014). For the groups with $M_h \lesssim 10^{13.5} h^{-1} M_\odot$, the stacked X-ray luminosity of the LC groups is significantly brighter than the HC groups at a given M_h.

X-ray emission of clusters/groups of galaxies has long been considered to reflect the dynamical status of group

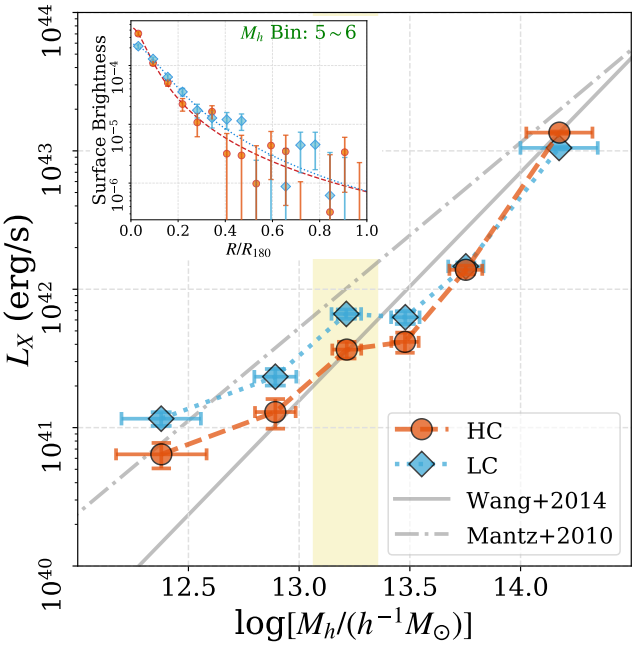

Figure 6. The stacked X-ray luminosity as a function of M_h for the HC (red) and LC (blue) groups. The vertical error bars show the errors transported from the uncertainties of the count rate and the horizontal error bars indicate the median deviation of the $\log\left[M_h/(h^{-1}M_\odot)\right]$ distribution in each bin. The solid and dashed-dotted lines represent the results obtained by Wang et al. (2014) and Mantz et al. (2010), respectively. The plot in the inset in the upper left corner presents an example of surface brightness profiles (symbols with error bars) with $\beta-$model fittings (lines) for stacks of HC (red) and LC (blue) groups in M_h Bin $= 5-6$, corresponding to the shaded region in the main plot.

systems. X-ray selected groups generally have lower late-type fractions than typical optically-selected ones and are known to be biased toward relaxed systems, particularly in the low-mass regime (e.g., Osmond & Ponman 2004; Eckert et al. 2011; Wen & Han 2013). Therefore, the systematically lower $L_{\rm X}$ for the HC groups, again, implies that they are potentially in a dynamical young status. To find further evidence of the correlation between the compactness of groups and their dynamical status, we investigate the star formation properties of individual galaxies living in groups with different compactness in the following section.

Besides the dynamical status, the X-ray emission of the intragroup medium is also known to be correlated with the feedback process of the radio AGN of the central galaxy (e.g., Shen et al. 2008). We will present a detailed study of the AGN phenomena in groups of galaxies with different compactness in section 5.2.

5. THE PROPERTIES OF GROUP MEMBER GALAXIES: DEPENDENCE ON GROUP COMPACTNESS

5.1. *Stellar Population of Galaxies*

We start by investigating the quenched fraction, which is defined as the fraction of galaxies that are quenched according to the aforementioned criterion of the HC and LC groups. Since our aim is to perform a fair comparison between the galaxies within the HC and LC groups at a given M_h, the bias due to different CLFs for these compared samples should be mitigated. The control samples for the HC and LC group galaxies are derived following the same method as described in section 4.2. Briefly, we match the central and satellite galaxies of the LC groups to those in the HC groups against the confounding covariates, $X_{\rm cen}$(or $X_{\rm sat}$) $= \{\log M_\star, z\}$ with a tolerance of $\{\Delta \log M_\star, \Delta z\} = \{0.2, 0.01\}$, respectively. The control samples derived in this way are referred to as control samples in the HC groups (HCS) and LC groups (LCS), respectively.

In figure 7, we first plot the quenched fraction as a function of M_h for the overall, central, and satellite population in three different panels, where the green solid and red dashed-dotted lines represent LCS and HCS, respectively. As a global trend, the quenched fraction increases systematically with M_h for each subsample. Since SDSS MGS is a flux-limited sample, the higher M_h systems are biased toward higher redshift than the lower M_h ones. Therefore, galaxies within higher M_h groups are on average more massive, so they have a higher quenched fraction (known as mass quenching). On the other hand, at a given $M_\star$, galaxies in higher M_h groups are also known to have a higher quenched fraction (known as halo quenching). Therefore, the systematically higher quenched fraction of galaxies in higher M_h bins we show in figure 7 is a combined result of both mass and halo quenching.

Besides the least massive M_h bin (we will discuss it later), we find that the relative quenched fraction for all galaxies in the LCS is systematically lower than that in the HCS, which mainly results from their systematically lower quenched fraction for satellite galaxies (the lower panel of figure 7). This result is in agreement with earlier findings that the galaxies in classical compact groups are on average redder than their counterparts living in noncompact groups (e.g., Coenda et al. 2012, 2015). On the other hand, recent studies (e.g., van den Bosch et al. 2008; Wetzel et al. 2012; Kauffmann et al. 2013; Wang et al. 2018) have found a dependency of galaxy quenching on halo-centric distance, where galaxies in central regions tend to be more quenched than their counter-

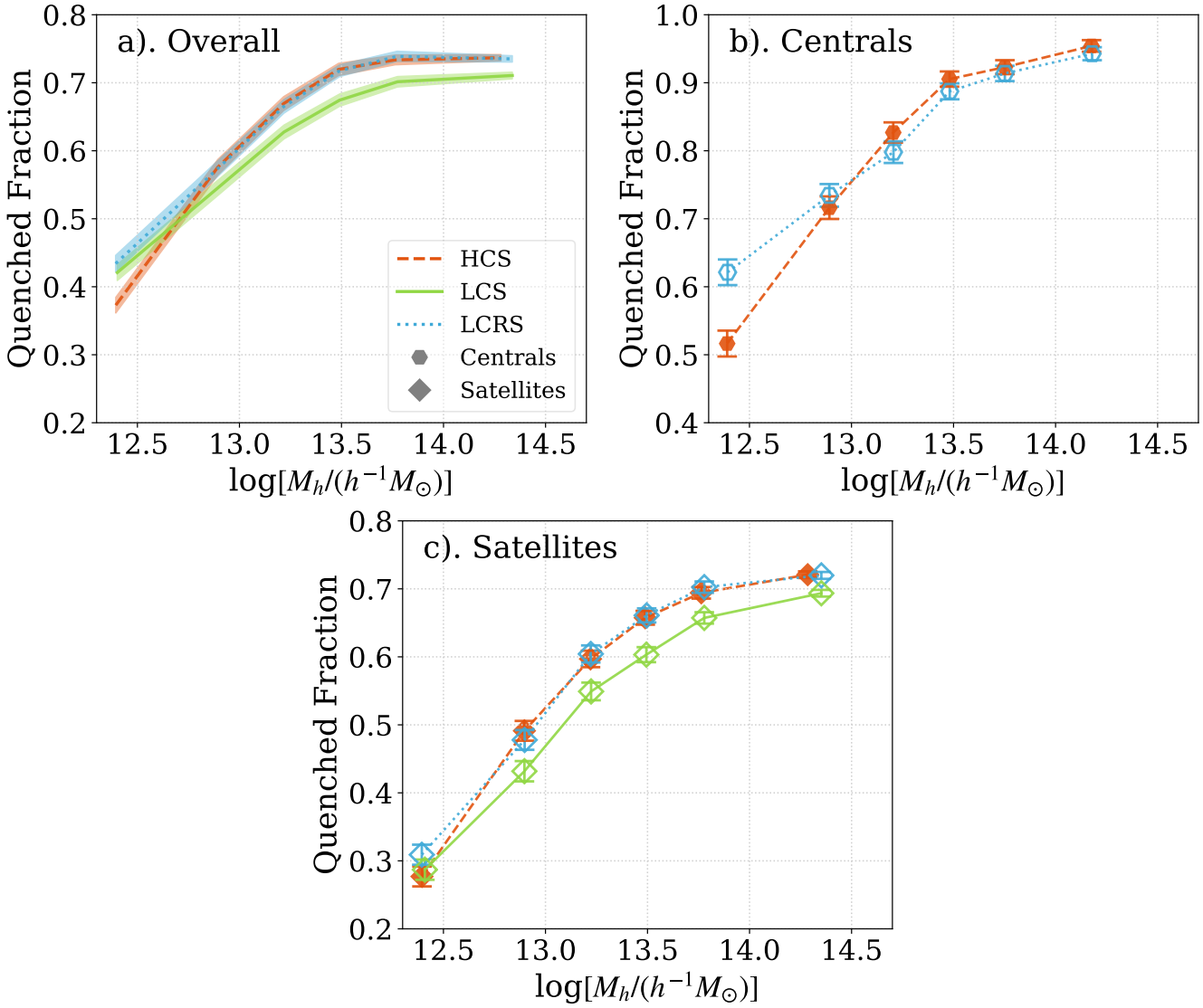

Figure 7. The quenched galaxy fraction for (a). overall, (b). central, and (c). satellite galaxies of the HCS (red), LCS (green), and LCRS (blue). Note that the central galaxies of LCS and LCRS are exactly the same; thus, we do not plot the results for the LCS in panel (b). In each panel, the errors in each bin represent the 68 percent confidence limits estimated using 1000 bootstrap resamplings.

parts in the outskirts. In our work, galaxies in the LCS and HSC have been controlled to have the same M_h so that have the same R_{180}. Therefore, the satellite galaxies of the HCS, by definition, naturally have systematically smaller R/R_{180} distributions than those of the LCS. That is to say, the systematically higher fraction of quenched galaxies in the HCS that we have found might be a result of their smaller average halo-centric distance.

To test this hypothesis, we construct another control sample of LC group galaxies, the central population of which remains unchanged, by matching the satellite population to those in the HCS with the confounding covariates, $X_{\rm sat} = \{\log M_\star, z, R/R_{180}\}$, scaled by a tolerance of $\{\Delta \log M_\star, \Delta z, \Delta R/R_{180}\} = \{0.2, 0.01, 0.025\}$. The control sample of LC groups derived in this way is referred to as the R-controlled sample in LC groups (LCRS). We plot the quenched fraction of galaxies for the LCRS as the blue dotted lines in each panel of figure 7.

We see that, for galaxies in the LC groups, when R/R_{180} is further controlled, the quenched fraction of satellite galaxies has systematically increases. The global quenched fraction of galaxies in the LCRS is now in excellent agreement with the galaxies in the HCS. This result implies that the halo quenching effect might be a faster process. In section 4, from the global properties of groups (e.g., magnitude gap, X-ray luminosity), we have argued that the HC groups are likely to be in the

early stage of group merging (or halo formation). Here, we see that although the HC groups are more likely to be recently formed, their members already show significant halo-centric dependence, i.e., galaxies in central regions of the halo are more likely to be quenched than in the outskirts.

On the other hand, although galaxies in the HCS and LCRS have been controlled to have the same R/R_{180} distributions, galaxies in the HCS actually still have systematically higher local density than those in the LCRS. The higher local density means that they are more likely to show a galaxy-galaxy interaction effect. Such an effect is manifested in the lowest M_h bin, where the local galaxy density (or $\mu_{\rm lim}$) of the HCS peaks (see also figure 1). For the least massive M_h bin where the halo quenching mechanism might not be very significant, we see a local galaxy-galaxy interaction effect, the galaxies in the HCS have systematically lower quenching fraction (because of enhanced star formation) than the LCS. Besides this bin, we see that the central galaxies in the HCS show a marginal increase in their proportion of quenched galaxies, this result might be affected by the magnitude measurement bias remaining in the pipeline, which we will discuss this in more detail in section 6.3.

5.2. *AGN Properties*

In the last section, we have shown that galaxies in the HCS have established a halo-centric relation as galaxies in the LCS. Here, we further explore whether the AGN phenomena of galaxies have been influenced by the formation phase of galaxy groups. To better control the variables, we focus on the HCS and LCRS only.

We show the fraction of optical AGN in central and satellite populations for the HCS and LCRS in the upper two panels of figure 8, where the left panel shows the fraction as a function of halo mass M_h, while the right panel shows that as a function of their stellar mass $M_\star$. We see that the global trend of optical AGN phenomena shows a complicated dependence on M_h and $M_\star$, which has been studied in detail by many previous works (e.g., Pasquali et al. 2009; Wang et al. 2018; Zhang et al. 2021). We give a brief overview here. First, the optical AGN phenomena peak around $M_\star \sim 10^{10.5-11} h^{-2} M_\odot$, and decreases with increasing M_h at $M_h \gtrsim 10^{12} h^{-1} M_\odot$. The central population has a higher fraction of optical AGNs than satellites at a given $M_\star$, which is due to the fact that the former live in the groups with lower M_h. On the other hand, the central galaxies show a higher average optical AGN fraction than satellites at a given M_h for $M_h \lesssim 10^{14} h^{-1} M_\odot$ because the former contains more $M_\star \sim 10^{10.5-11} h^{-2} M_\odot$ galaxies. In addition to these known overall trends, for subsamples of the HCS and LCRS, we do not see any systematic differences between the HCS and LCRS.

For radio-AGN phenomena, owing to the fact that radio-loud AGN are not very abundant, and Wang et al. (2018) showed that there is no difference in radio properties between central and satellite galaxies at given M_h and $M_\star$, we do not separate the galaxies into central and satellite populations here. In the lower panels of figure 8, we show the radio-loud AGN fraction for all galaxies in the HCS and LCRS as a function of $M_\star$ (left) and M_h (right), respectively. We also do not see any significant differences between the galaxies in HCS and LCRS. However, it is worth mentioning that the radio-loud AGN fraction of small satellites in the HCS sample seems systematically higher than that of their counterparts in the LCRS. Such a difference is interesting but suspicious since we know that the radio-loud AGN phenomena is linked with super-massive black holes which generally live in massive galaxies. This suspiciously higher radio-loud fraction at the low $M_\star$ end might come from the contamination during the identification of radio-loud AGN. An FR-II galaxy have two radio lobes separated out to a distance of $\sim$ 100 kpc, which is very likely to contaminate its neighbors if this radio galaxy is located in a higher density region like the HC groups (Best et al. 2005). A detailed study of the origin of this systematical difference is beyond the scope of this paper and deserves to be carried out in the future.

In summary, we find no systematic differences in AGN phenomena between the galaxies in the HCS and LCRS when their halo-centric effect has also been controlled. This result is consistent with an earlier finding that there is no dependence on optical nuclear activity within the local environment of galaxies (e.g., Argudo-Fernández et al. 2016).

6. DISCUSSION

So far, we have used a carefully controlled sample and quantitative statistical methods to investigate how properties of a galaxy group and its galaxy members depend on its structure parameter: group compactness. However, there are still some biases remaining in the data analysis pipeline, which could potentially affect our results. In this section, we further discuss on these issues and present the robustness of our results.

6.1. *Redshift Incompleteness*

As mentioned in section 2.1, redshift incompleteness are more frequently occurred in the HC groups, figure 9 presents the redshift completeness as a function of M_h for the HC, IC, and LC groups. A trend of increasing

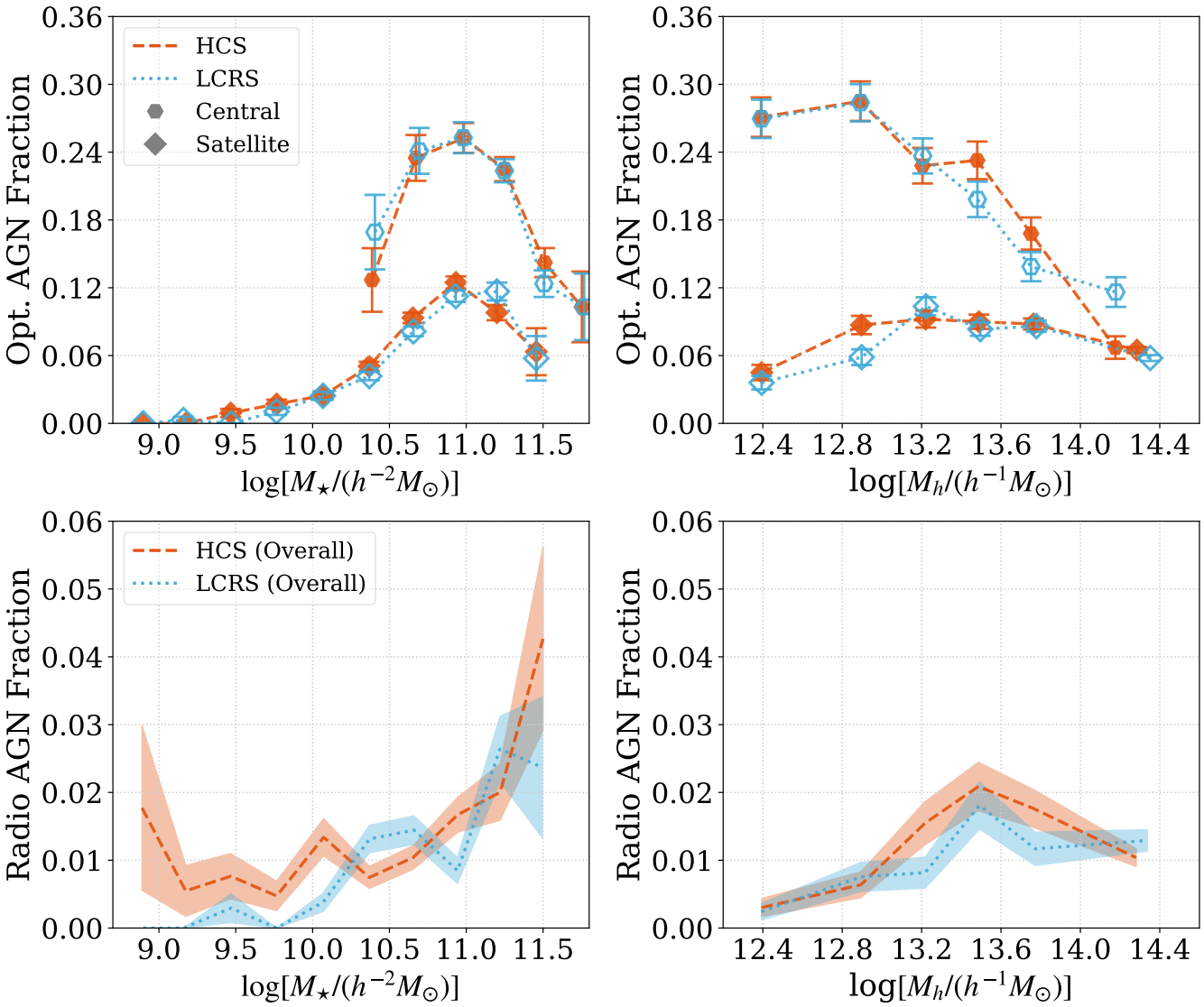

Figure 8. Upper Panel: The optical AGN fraction for central (hexagon) and satellite (diamond) galaxies of the HCS (red) and LCRS (blue), respectively. Lower Panel: The radio-loud AGN fraction for all galaxies of the HCS and LCRS. In each subplot, the errors in each bin represent the 68 percent confidence limits estimated using 1000 bootstrap resamplings.

redshift incompleteness with decreasing M_h is clearly seen for the HC groups, while there is no such trend for the IC and LC groups. This systematic trend is a result of increasing compactness limit for the selection of HC groups in low M_h bins (figure 1), where the fiber collision effect is easier to be trigger.

In our study, we have assigned redshifts from their nearest neighbor for these galaxies without any spectroscopic redshifts. That is to say, there is a larger fraction of galaxies in the HC groups being contaminated by foreground or background galaxies, which biases the M_h estimation of HC groups to higher values. This bias introduces a question on our results in section 4.3, where we have shown that the HC groups have systematically fainter X-ray luminosities than LC groups at lower M_h bins. In section 2, we show that $\sim$ 65% of the spectroscopy of unmeasured galaxies are genuine members of their assigned groups. Therefore, we do not expect that this redshift incompleteness bias on M_h estimation will be significant. For the lowest M_h bin with the most serious incompleteness problem, the redshift completeness of the HC groups is $\sim$ 78%, which results in an over-estimation of M_h for the HC groups at the level of $\sim$ 0.03 dex, much smaller than the bin width ($\sim$ 0.63 dex). Such a small difference in M_h obviously can not account for the difference in $L_{\rm X}$ between the low-mass HC and LC groups ($\sim$ 0.3 dex) we have obtained in section 2.

Besides the global bias, as shown by the subplots in the inset of figure 9, the redshift incompleteness is not

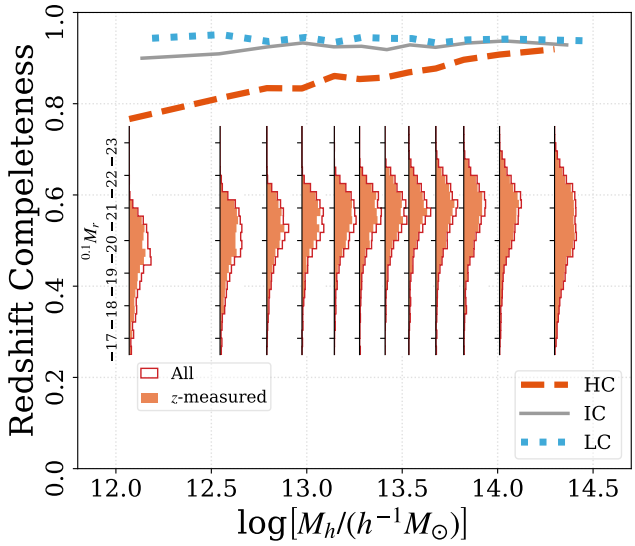

Figure 9. Redshift completeness for galaxies living in the HC (red dashed), IC (grey solid), and LC (blue dotted) groups as a function of M_h. The insets represent the $^{0.1}M_r$ distributions for the HC group galaxies with (filled) or without (open) redshift measurement in each M_h bin.

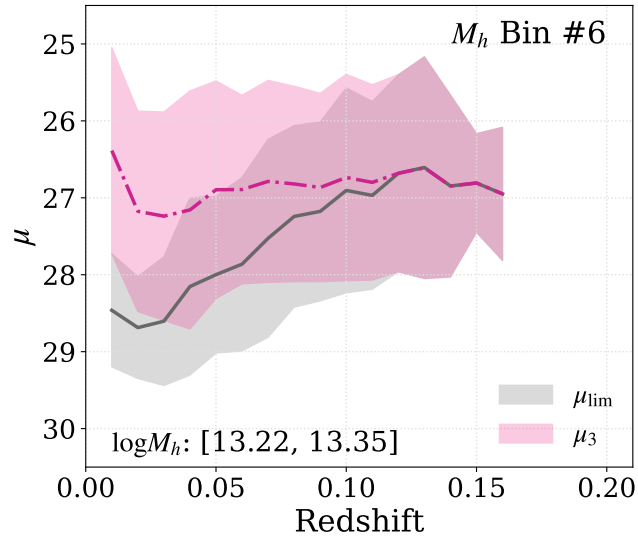

Figure 10. An example of the median and scatter of $\mu_{\rm lim}$ (grey) and μ_3 (magenta) as a function of redshift for Y07 groups in the M_h Bin = 6.

uniform, but clearly biased toward fainter (or satellite) galaxies. For instance, the redshift completeness of the central galaxies and satellites of HC groups in the lowest M_h bin are $\sim 87\%$ and $\sim 72\%$, respectively.[2] This non-uniform bias in magnitude might have an impact on the CLF and magnitude gap studies in section 4.

To further validate our results presented in section 4 compared with the redshift incompleteness, we use a smaller but cleaner subsample for the robustness test. To do that, we remove the groups with member completeness $\leq 80\%$ to ensure that low richness ($3 \leq N \leq 5$) groups have 100% completeness and the bias on M_h estimation for the high richness groups ($N \geq 6$) are negligible [3]. After removing $\sim 5,500$ groups not satisfying with this condition, we repeat all the studies in section 4 and find consistent results inside statistical errors.

Finally, during the study of the properties of group member galaxies in section 5, we only use the galaxies with spectroscopic measurements in SDSS-DR7 and make comparisons using carefully selected control samples. Therefore, we do not expect any biases to be produced by the redshift incompleteness here.

6.2. *Alternative Compactness Definition: μ_N*

Historically, Hickson (1982) originally used a fixed value of $\mu_{\rm lim} = 26.0$ mag arcsec^{-2} to define the classical compact groups. However, as mentioned in section 2.1, the $\mu_{\rm lim}$ distribution shows a clear dependence on redshift. This redshift bias might be due to the fact that galaxies within groups are not randomly distributed. The brighter galaxy members suffer the dynamical friction effect more significantly and are on average located in more central regions (Saro et al. 2013). The faint members in the outskirts are more likely to be out of the detection limit in the flux limit sample, which makes the $\mu_{\rm lim}$ measurement be biased toward lower values for higher redshift groups. Therefore, using a fixed value of $\mu_{\rm lim}$ as the compact group threshold will result in an in-homogeneous sample at different redshifts (Zheng & Shen 2020). One option that might alleviate this redshift bias is adopting an alternative compactness definition, μ_N, based on the brightest N galaxy members.

Here, we use μ_3, the surface brightness as given by Equation (1) but calculated using the three brightest galaxies only, to test our hypothesis. We show an example of the μ_3−redshift relation for groups in M_h Bin= 6 in figure 10. Clearly, the redshift dependence is significantly reduced, and the quartile values show little change with redshift. On the other hand, using fewer galaxy members to calculate μ_N leads to a larger random dispersion on group compactness. As can be seen in figure 10, the scatter of μ_3 is about 2 times larger than $\mu_{\rm lim}$ at low redshift. At high redshift, because of the decreasing of the observable members, μ_3 becomes to be equivalent to $\mu_{\rm lim}$. We have tested, using μ_3 in-

[2] This less significant bias might stem from the fact that the brighter galaxies more easily obtain spectroscopic reshifts from the LAMOST spectral survey easier (Shen et al. 2016).

[3] Most of the groups with $M_h \lesssim 10^{13.5} h^{-1} M_\odot$ have richness $3 \leq N \leq 5$.

stead of $\mu_{\rm lim}$ to define the HC and LC groups, and all of our conclusions remain unchanged but with much lower significance.

6.3. *Magnitude Measurement of Galaxies in the High Density Region*

The magnitude measurement of galaxies in the high density region is known to be easily biased to high values, i.e., underestimation of the flux because of the difficulties in the subtraction of background (e.g, Lauer et al. 2007; Von Der Linden et al. 2007).

For our HC groups, the surface brightness is as high as $\mu_{\rm lim} \sim 26$ mag arcsec^{-2}, where the magnitude measurement bias very likely happens. If so, the stellar masses of galaxy members of the HC groups, especially for the central population, will be underestimated. Such an underestimation effect might account for the systematically higher (although not significant) quenching fraction of central galaxies within higher M_h HC groups. On the other hand, because of the underestimation of $M_\star$, M_h will also be underestimated. Such an underestimation effect on M_h might compensate for the overestimation effect discussed in section 6.1.

7. CONCLUSION

In this study, we have performed a systematic and statistical analysis of the compactness of galaxy groups based on an $N \geq 3$ group sample drawn from the halo-based group catalog of Yang et al. (2007) as well as the extra GAMA and LAMOST redshift measurements. Based on the group surface brightness $\mu_{\rm lim}$, the total luminosity averaged over the smallest circle enclosing all the members, akin to the compactness criterion for classical compact groups introduced by Hickson (1982), we divide the samples into the HC and LC groups based on the aggregate relation of $\mu_{\rm lim}$ versus redshift in each M_h bin. We investigate various aspects of the individual and global properties such as CLF, Δm_{12}, X-ray luminosity of ICM, quenched fraction and AGN fraction. We reach the following conclusions and predictions:

1. For massive halos ($M_h \gtrsim 10^{13.5} h^{-1} M_\odot$), there is no significant dependence on group compactness. Also, at the same redshift, massive groups are generally less compact (higher $\mu_{\rm lim}$) than small groups in observation. This echoes the fact that the classical compact groups are generally small galaxy systems (e.g., McConnachie et al. 2009; Zheng & Shen 2020).

2. The HC groups are generally comprised of several members with comparable $M_\star$ (or luminosity), while the LC groups generally contain a more dominant central galaxy. This is relevant to the studies of fossil groups, such as the studies by Farhang et al. (2017) and Raouf et al. (2019), which have suggested that the fossil groups with a larger magnitude gap Δm_{12} tend to be older and the spatial distribution of their galaxy members are less crowded compared to the non-relaxed groups. Combined with the fact that the average X-ray luminosity of the LC groups is higher than the HC ones in the range of $M_h \lesssim 10^{13.5} h^{-1} M_\odot$, we argue that those small HC groups, on average, are in the early stages of group merging.

3. The HC groups contain more passive galaxies than the LC groups with similar M_h at a given $M_\star$, which is a result of their different halo-centric distance distributions for a satellite population. When controlled for halo-centric distance further, this difference tends to disappear. We conclude that the halo quenching effect in galaxy members, which makes the dependence of passive fraction on halo-centric distance, is a faster process compared to the dynamical relaxing time-scale for the groups in which they are hosted.

4. The fraction of galaxies that host an optical or radio-loud AGN depends weakly on group compactness, indicating the local environmental effect triggered by group evolution does not correlate with the AGN activity of galaxies.

In summary, our results imply a relationship between the observed group compactness and halo formation history. However, this relationship is not consistent with the inferences obtained from simulations of pure dark matter halo, where the halos with higher concentration are believed to be formed earlier (e.g., Zhao et al. 2009; Ragagnin et al. 2019). To further clarify the possible inconsistency between our observations and numerical simulations, we need a joint effort for both. On the one hand, by expanding to a larger and deeper galaxy sample (e.g., DESI, Dark Energy Survey Collaboration et al. 2016), we would expand the definition of group compactness to include more fainter group members. On the other hand, cosmological simulations including both dark matter and baryonic components (e.g., IllustrisTNG, Pillepich et al. 2018) are helpful for resolving the formation histories of groups with different group compactness and exploring the relationship between halo concentration and group compactness.

ACKNOWLEDGEMENTS

We acknowledge the anonymous referee for helpful comments and detailed suggestions. This work is

supported by National Key R&D Program of China No.2019YFA0405501 and the National Natural Science Foundation of China (grant No. 12073059, 12103017).

This work has made use of data products from the Sloan Digital Sky Survey (SDSS, http://www.sdss.org), the Large Sky Area Multi-Object Fiber Spectroscopic Telescope (LAMOST, http://www.lamost.org), the GAMA survey (http://www.gama-survey.org. We are thankful for their tremendous efforts on the surveying work.

The Guoshoujing Telescope (the Large Sky Area Multi-Object Fiber Spectroscopic Telescope LAMOST) is a National Major Scientific Project built by the Chinese Academy of Sciences. Funding for the project has been provided by the National Development and Reform Commission. LAMOST is operated and managed by the National Astronomical Observatories, Chinese Academy of Sciences.

REFERENCES

Abazajian, K. N., Adelman-McCarthy, J. K., Agüeros, M. A., et al. 2009, ApJS, 182, 543. doi:10.1088/0067-0049/182/2/543

Ahumada, R., Prieto, C. A., Almeida, A., et al. 2020, ApJS, 249, 3. doi:10.3847/1538-4365/ab929e

Amram, P., Mendes de Oliveira, C., Plana, H., et al. 2004, ApJL, 612, L5. doi:10.1086/424482

Argudo-Fernández, M., Shen, S., Sabater, J., et al. 2016, A&A, 592, A30. doi:10.1051/0004-6361/201628232

Baldwin, J. A., Phillips, M. M., & Terlevich, R. 1981, PASP, 93, 5. doi:10.1086/130766

Barnes, J. E. 1989, Nature, 338, 123. doi:10.1038/338123a0

Barton, E., Geller, M., Ramella, M., Marzke, R. O., & da Costa, L. N. 1996, AJ, 112, 871

Becker, R. H., White, R. L., & Helfand, D. J. 1995, ApJ, 450, 559. doi:10.1086/176166

Bell, E. F., McIntosh, D. H., Katz, N., et al. 2003, ApJS, 149, 289. doi:10.1086/378847

Best, P. N., Kauffmann, G., Heckman, T. M., et al. 2005, MNRAS, 362, 25. doi:10.1111/j.1365-2966.2005.09192.x

Best, P. N. & Heckman, T. M. 2012, MNRAS, 421, 1569. doi:10.1111/j.1365-2966.2012.20414.x

Blanton, M. R., Schlegel, D. J., Strauss, M. A., et al. 2005, AJ, 129, 2562

Bluck, A. F. L., Mendel, J. T., Ellison, S. L., et al. 2014, MNRAS, 441, 599. doi:10.1093/mnras/stu594

Bluck, A. F. L., Mendel, J. T., Ellison, S. L., et al. 2016, MNRAS, 462, 2559. doi:10.1093/mnras/stw1665

Briel, U. G., Aschenbach, B., Hasinger, G., et al. 1996, The ROSAT Users' Handbook. A guide to the Astronomical X-Ray satellite ROSAT. Intended to provide ROSAT users with an overview of all technical aspects of ROSAT. With special emphasis on the calibration of the various instruments. Garching bei Muenchen, 1996. 212 pages.

Brinchmann, J., Charlot, S., White, S. D. M., et al. 2004, MNRAS, 351, 1151. doi:10.1111/j.1365-2966.2004.07881.x

Böhringer, H., Voges, W., Huchra, J. P., et al. 2000, ApJS, 129, 435. doi:10.1086/313427

Böhringer, H., Schuecker, P., Guzzo, L., et al. 2004, A&A, 425, 367. doi:10.1051/0004-6361:20034484

Charlot, S. & Fall, S. M. 2000, ApJ, 539, 718. doi:10.1086/309250

Cid Fernandes, R., Stasińska, G., Schlickmann, M. S., et al. 2010, MNRAS, 403, 1036. doi:10.1111/j.1365-2966.2009.16185.x

Cid Fernandes, R., Stasińska, G., Mateus, A., et al. 2011, MNRAS, 413, 1687. doi:10.1111/j.1365-2966.2011.18244.x

Cluver, M. E., Jarrett, T. H., Taylor, E. N., et al. 2020, arXiv:2006.07535

Coenda, V., Muriel, H., & Martínez, H. J. 2012, A&A, 543, A119

Coenda, V., Muriel, H., & Martínez, H. J. 2015, A&A, 573, A96. doi:10.1051/0004-6361/201424870

Condon, J. J., Cotton, W. D., Greisen, E. W., et al. 1998, AJ, 115, 1693. doi:10.1086/300337

Cooray, A. 2006, MNRAS, 365, 842. doi:10.1111/j.1365-2966.2005.09747.x

Coziol, R. & Plauchu-Frayn, I. 2007, AJ, 133, 2630. doi:10.1086/513514

Croton, D. J., Springel, V., White, S. D. M., et al. 2006, MNRAS, 365, 11. doi:10.1111/j.1365-2966.2005.09675.x

Cui, W., Davé, R., Peacock, J. A., et al. 2021, Nature Astronomy. doi:10.1038/s41550-021-01404-1

Dai, X., Kochanek, C. S., & Morgan, N. D. 2007, ApJ, 658, 917. doi:10.1086/509651

Dariush, A. A., Raychaudhury, S., Ponman, T. J., et al. 2010, MNRAS, 405, 1873. doi:10.1111/j.1365-2966.2010.16569.x

Dark Energy Survey Collaboration, Abbott, T., Abdalla, F. B., et al. 2016, MNRAS, 460, 1270. doi:10.1093/mnras/stw641

Davies, L. J. M., Robotham, A. S. G., Lagos, C. del P., et al. 2019, MNRAS, 483, 5444. doi:10.1093/mnras/sty3393

Dekel, A. & Birnboim, Y. 2006, MNRAS, 368, 2. doi:10.1111/j.1365-2966.2006.10145.x
Díaz-Giménez, E. & Zandivarez, A. 2015, A&A, 578, A61. doi:10.1051/0004-6361/201425267
Díaz-Giménez, E., Zandivarez, A., & Taverna, A. 2018, A&A, 618, A157. doi:10.1051/0004-6361/201833329
Dickey, J. M. & Lockman, F. J. 1990, ARA&A, 28, 215. doi:10.1146/annurev.aa.28.090190.001243
Eckert, D., Molendi, S., & Paltani, S. 2011, A&A, 526, A79. doi:10.1051/0004-6361/201015856
Efstathiou, G., Ellis, R. S., & Peterson, B. A. 1988, MNRAS, 232, 431
Fabian, A. C. 2012, ARA&A, 50, 455. doi:10.1146/annurev-astro-081811-125521
Farhang, A., Khosroshahi, H. G., Mamon, G. A., et al. 2017, ApJ, 840, 58. doi:10.3847/1538-4357/aa6b00
Farouki, R., & Shapiro, S. L. 1981, ApJ, 243, 32
Feng, S., Shen, S.-Y., Yuan, F.-T., et al. 2019, ApJ, 880, 114
Gunn, J. E., & Gott, J. R. 1972, ApJ, 176, 1
Guo, Q., White, S., Li, C., et al. 2010, MNRAS, 404, 1111. doi:10.1111/j.1365-2966.2010.16341.x
Haas, M. R., Schaye, J., & Jeeson-Daniel, A. 2012, MNRAS, 419, 2133. doi:10.1111/j.1365-2966.2011.19863.x
Harrison, C. M. 2017, Nature Astronomy, 1, 0165. doi:10.1038/s41550-017-0165
Henriques, B. M. B., White, S. D. M., Thomas, P. A., et al. 2017, MNRAS, 469, 2626. doi:10.1093/mnras/stx1010
Hickson, P. 1982, ApJ, 255, 382
Jiang, C. Y., Jing, Y. P., & Han, J. 2014, ApJ, 790, 7. doi:10.1088/0004-637X/790/1/7
Jing, Y. P., Mo, H. J., & Börner, G. 1998, ApJ, 494, 1. doi:10.1086/305209
Kauffmann, G., Heckman, T. M., White, S. D. M., et al. 2003, MNRAS, 341, 33. doi:10.1046/j.1365-8711.2003.06291.x
Kauffmann, G., Heckman, T. M., Tremonti, C., et al. 2003, MNRAS, 346, 1055. doi:10.1111/j.1365-2966.2003.07154.x
Kauffmann, G., White, S. D. M., Heckman, T. M., et al. 2004, MNRAS, 353, 713. doi:10.1111/j.1365-2966.2004.08117.x
Kauffmann, G., Li, C., Zhang, W., et al. 2013, MNRAS, 430, 1447. doi:10.1093/mnras/stt007
Kewley, L. J., Dopita, M. A., Sutherland, R. S., et al. 2001, ApJ, 556, 121. doi:10.1086/321545
Khosroshahi, H. G., Raouf, M., Miraghaei, H., et al. 2017, ApJ, 842, 81. doi:10.3847/1538-4357/aa7048
Knobel, C., Lilly, S. J., Woo, J., et al. 2015, ApJ, 800, 24. doi:10.1088/0004-637X/800/1/24
Koester, B. P., McKay, T. A., Annis, J., et al. 2007, ApJ, 660, 239. doi:10.1086/509599
Kravtsov, A. V., Berlind, A. A., Wechsler, R. H., et al. 2004, ApJ, 609, 35. doi:10.1086/420959
Lange, J. U., van den Bosch, F. C., Hearin, A., et al. 2018, MNRAS, 473, 2830. doi:10.1093/mnras/stx2434
Lauer, T. R., Faber, S. M., Richstone, D., et al. 2007, ApJ, 662, 808. doi:10.1086/518223
Li, C., Kauffmann, G., Jing, Y. P., et al. 2006, MNRAS, 368, 21. doi:10.1111/j.1365-2966.2006.10066.x
Li, P., Wang, H., Mo, H. J., et al. 2020, ApJ, 902, 75. doi:10.3847/1538-4357/abb66c
Li, Z. & Cen, R. 2020, ApJ, 898, 39. doi:10.3847/1538-4357/ab9811
Liske, J., Baldry, I. K., Driver, S. P., et al. 2015, MNRAS, 452, 2087
Liu, L., Yang, X., Mo, H. J., et al. 2010, ApJ, 712, 734. doi:10.1088/0004-637X/712/1/734
Liu, C., Hao, L., Wang, H., et al. 2019, ApJ, 878, 69. doi:10.3847/1538-4357/ab1ea0
Lovisari, L., Ettori, S., Gaspari, M., et al. 2021, Universe, 7, 139. doi:10.3390/universe7050139
Lu, Z., Mo, H. J., Lu, Y., et al. 2014, MNRAS, 439, 1294. doi:10.1093/mnras/stu016
Luo, A.-L., Zhao, Y.-H., Zhao, G., et al. 2015, Research in Astronomy and Astrophysics, 15, 1095
Mamon, G. 1993, N-body Problems and Gravitational Dynamics, 188
Mamon, G. A. 2007, Groups of Galaxies in the Nearby Universe, 203
Mandelbaum, R., Wang, W., Zu, Y., et al. 2016, MNRAS, 457, 3200. doi:10.1093/mnras/stw188
Mantz, A., Allen, S. W., Ebeling, H., et al. 2010, MNRAS, 406, 1773. doi:10.1111/j.1365-2966.2010.16993.x
Martínez, H. J. & Zandivarez, A. 2012, MNRAS, 419, L24. doi:10.1111/j.1745-3933.2011.01170.x
Matthee, J., Schaye, J., Crain, R. A., et al. 2017, MNRAS, 465, 2381. doi:10.1093/mnras/stw2884
McConnachie, A. W., Patton, D. R., Ellison, S. L., & Simard, L. 2009, MNRAS, 395, 255
Mendel, J. T., Ellison, S. L., Simard, L., Patton, D. R., & McConnachie, A. W. 2011, MNRAS, 418, 1409
Mo, H. J., Mao, S., & White, S. D. M. 1999, MNRAS, 304, 175. doi:10.1046/j.1365-8711.1999.02289.x
Moore, B., Katz, N., Lake, G., Dressler, A., & Oemler, A. 1996, Nature, 379, 613
More, S., van den Bosch, F. C., Cacciato, M., et al. 2011, MNRAS, 410, 210. doi:10.1111/j.1365-2966.2010.17436.x
More, S. 2012, ApJ, 761, 127. doi:10.1088/0004-637X/761/2/127
Moster, B. P., Naab, T., & White, S. D. M. 2018, MNRAS, 477, 1822. doi:10.1093/mnras/sty655

Osmond, J. P. F. & Ponman, T. J. 2004, MNRAS, 350, 1511. doi:10.1111/j.1365-2966.2004.07742.x

Osterbrock, D. E. 1989, Astrophysics of Gaseous Nebulae and Active Galactic Nuclei, by Donald E. Osterbrock. Published by University Science Books, ISBN 0-935702-22-9, 408pp, 1989.

Paranjape, A. & Sheth, R. K. 2012, MNRAS, 423, 1845. doi:10.1111/j.1365-2966.2012.21008.x

Pasquali, A., van den Bosch, F. C., Mo, H. J., et al. 2009, MNRAS, 394, 38. doi:10.1111/j.1365-2966.2008.14233.x

Peacock, J. A. & Smith, R. E. 2000, MNRAS, 318, 1144. doi:10.1046/j.1365-8711.2000.03779.x

Peng, Y.-. jie ., Lilly, S. J., Kovač, K., et al. 2010, ApJ, 721, 193. doi:10.1088/0004-637X/721/1/193

Peng, Y.-. jie ., Lilly, S. J., Renzini, A., et al. 2012, ApJ, 757, 4. doi:10.1088/0004-637X/757/1/4

Peng, Y.-. jie ., Lilly, S. J., Renzini, A., et al. 2014, ApJ, 790, 95. doi:10.1088/0004-637X/790/2/95

Pillepich, A., Springel, V., Nelson, D., et al. 2018, MNRAS, 473, 4077. doi:10.1093/mnras/stx2656

Ragagnin, A., Dolag, K., Moscardini, L., et al. 2019, MNRAS, 486, 4001. doi:10.1093/mnras/stz1103

Raouf, M., Khosroshahi, H. G., Ponman, T. J., et al. 2014, MNRAS, 442, 1578. doi:10.1093/mnras/stu963

Raouf, M., Khosroshahi, H. G., Mamon, G. A., et al. 2018, ApJ, 863, 40. doi:10.3847/1538-4357/aace57

Raouf, M., Smith, R., Khosroshahi, H. G., et al. 2019, ApJ, 887, 264. doi:10.3847/1538-4357/ab5581

Reddick, R. M., Wechsler, R. H., Tinker, J. L., et al. 2013, ApJ, 771, 30. doi:10.1088/0004-637X/771/1/30

Robotham, A. S. G., Norberg, P., Driver, S. P., et al. 2011, MNRAS, 416, 2640. doi:10.1111/j.1365-2966.2011.19217.x

Saro, A., Mohr, J. J., Bazin, G., et al. 2013, ApJ, 772, 47. doi:10.1088/0004-637X/772/1/47

Schechter, P. 1976, ApJ, 203, 297

Shen, S., Kauffmann, G., von der Linden, A., et al. 2008, MNRAS, 389, 1074. doi:10.1111/j.1365-2966.2008.13647.x

Shen, S., Yang, X., Mo, H., et al. 2014, ApJ, 782, 23. doi:10.1088/0004-637X/782/1/23

Shen, S.-Y., Argudo-Fernández, M., Chen, L., et al. 2016, Research in Astronomy and Astrophysics, 16, 43

Simha, V., Weinberg, D. H., Davé, R., et al. 2012, MNRAS, 423, 3458. doi:10.1111/j.1365-2966.2012.21142.x

Sohn, J., Hwang, H. S., Geller, M. J., et al. 2015, Journal of Korean Astronomical Society, 48, 381

Sohn, J., Geller, M. J., Hwang, H. S., Zahid, H. J., & Lee, M. G. 2016, ApJS, 225, 23

Stewart, K. R., Bullock, J. S., Barton, E. J., et al. 2009, ApJ, 702, 1005. doi:10.1088/0004-637X/702/2/1005

Tal, T., Wake, D. A., van Dokkum, P. G., et al. 2012, ApJ, 746, 138. doi:10.1088/0004-637X/746/2/138

Tammann, G. A., Yahil, A., & Sandage, A. 1979, ApJ, 234, 775

Torres-Flores, S., Mendes de Oliveira, C., de Mello, D. F., et al. 2009, A&A, 507, 723. doi:10.1051/0004-6361/200911878

Torres-Flores, S., Mendes de Oliveira, C., Amram, P., et al. 2010, A&A, 521, A59. doi:10.1051/0004-6361/200913912

Torres-Flores, S., Amram, P., Mendes de Oliveira, C., et al. 2014, MNRAS, 442, 2188. doi:10.1093/mnras/stu1002

Trevisan, M. & Mamon, G. A. 2017, MNRAS, 471, 2022. doi:10.1093/mnras/stx1656

Vale, A. & Ostriker, J. P. 2006, MNRAS, 371, 1173. doi:10.1111/j.1365-2966.2006.10605.x

van den Bosch, F. C., Yang, X., Mo, H. J., et al. 2007, MNRAS, 376, 841. doi:10.1111/j.1365-2966.2007.11493.x

van den Bosch, F. C., Pasquali, A., Yang, X., et al. 2008, arXiv:0805.0002

Voges, W., Aschenbach, B., Boller, T., et al. 1999, A&A, 349, 389

Von Der Linden, A., Best, P. N., Kauffmann, G., et al. 2007, MNRAS, 379, 867. doi:10.1111/j.1365-2966.2007.11940.x

Wang, L., Yang, X., Shen, S., et al. 2014, MNRAS, 439, 611. doi:10.1093/mnras/stt2481

Wang, E., Wang, H., Mo, H., et al. 2018, ApJ, 860, 102. doi:10.3847/1538-4357/aac4a5

Weinmann, S. M., van den Bosch, F. C., Yang, X., et al. 2006, MNRAS, 366, 2. doi:10.1111/j.1365-2966.2005.09865.x

Wen, Z. L. & Han, J. L. 2013, MNRAS, 436, 275. doi:10.1093/mnras/stt1581

Wetzel, A. R., Tinker, J. L., & Conroy, C. 2012, MNRAS, 424, 232. doi:10.1111/j.1365-2966.2012.21188.x

White, D. A., Jones, C., & Forman, W. 1997, MNRAS, 292, 419. doi:10.1093/mnras/292.2.419

Woo, J., Dekel, A., Faber, S. M., et al. 2013, MNRAS, 428, 3306. doi:10.1093/mnras/sts274

Woo, J., Dekel, A., Faber, S. M., et al. 2015, MNRAS, 448, 237. doi:10.1093/mnras/stu2755

Yang, X., Mo, H. J., & van den Bosch, F. C. 2003, MNRAS, 339, 1057. doi:10.1046/j.1365-8711.2003.06254.x

Yang, X., Mo, H. J., van den Bosch, F. C., et al. 2005, MNRAS, 356, 1293

Yang, X., Mo, H. J., van den Bosch, F. C., et al. 2007, ApJ, 671, 153

Yang, X., Mo, H. J., & van den Bosch, F. C. 2008, ApJ, 676, 248. doi:10.1086/528954

Yang, X., Mo, H. J., van den Bosch, F. C., et al. 2012, ApJ, 752, 41

Yang, X., Mo, H. J., van den Bosch, F. C., et al. 2013, ApJ, 770, 115. doi:10.1088/0004-637X/770/2/115

Yang, X., Xu, H., He, M., et al. 2021, ApJ, 909, 143. doi:10.3847/1538-4357/abddb2

Zehavi, I., Contreras, S., Padilla, N., et al. 2018, ApJ, 853, 84. doi:10.3847/1538-4357/aaa54a

Zhang, C., Peng, Y., Ho, L. C., et al. 2021, ApJ, 911, 57. doi:10.3847/1538-4357/abd723

Zhang, Z., Wang, H., Luo, W., et al. 2021, A&A, 650, A155. doi:10.1051/0004-6361/202040150

Zhao, D. H., Jing, Y. P., Mo, H. J., et al. 2009, ApJ, 707, 354. doi:10.1088/0004-637X/707/1/354

Zheng, Y.-L., & Shen, S.-Y. 2020, ApJS, 246, 12

Zheng, Y.-L. & Shen, S.-Y. 2021, ApJ, 911, 105. doi:10.3847/1538-4357/abeaa2

Zheng, Z., Berlind, A. A., Weinberg, D. H., et al. 2005, ApJ, 633, 791. doi:10.1086/466510

Zu, Y. & Mandelbaum, R. 2016, MNRAS, 457, 4360. doi:10.1093/mnras/stw221